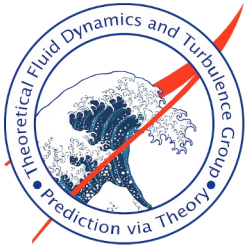

Fully-Parabolized Prediction of Hypersonic Sonic Boom

Christian B. King, Sean M. Skowron, and Steven A. E. Miller

University of Florida

Department of Mechanical and Aerospace Engineering

Theoretical Fluid Dynamics and Turbulence Group

christianking@ufl.edu

https://faculty.eng.ufl.edu/fluids

Acknowledgements

Research was sponsored by the Defense Advanced Research Project Agency (DARPA) and the Army Research Office and was accomplished under Grant Number W911NF-21-1-0342. The views and conclusions contained in this document are those of the authors and should not be interpreted as representing the official policies, either expressed or implied, of the Army Research Office or the U.S. Government. The U.S. Government is authorized to reproduce and distribute reprints for Government purposes notwithstanding any copyright notation herein.

Background

- Hypersonic vehicles produce shock and expansion waves that radiate to the ground and are heard as a sonic boom
- Non-equilibrium flow and viscous effects on sonic boom are not well understood
- Understanding these phenomena is essential for accurate sonic boom prediction

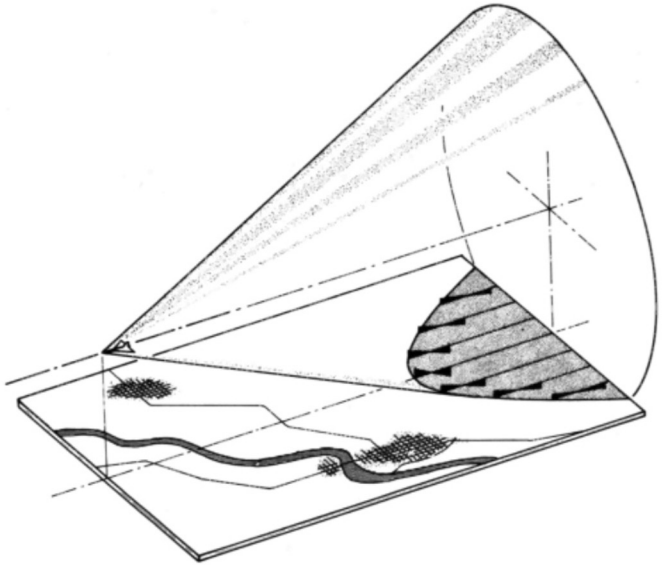

Fig. 1. Carlson, Acoustical Society of America, 1972 [1].

State-of-the-Art in Near-Field Prediction

- NASA's FUN3D solver with adjoint-based mesh adaptation (Park, AIAAJ, 2004 [2])
- Incorporates LAURA's high-energy physics suite.
- Faster, more accurate results; however, large computational expense
- Other state-of-the-art approaches include the LAVA framework and

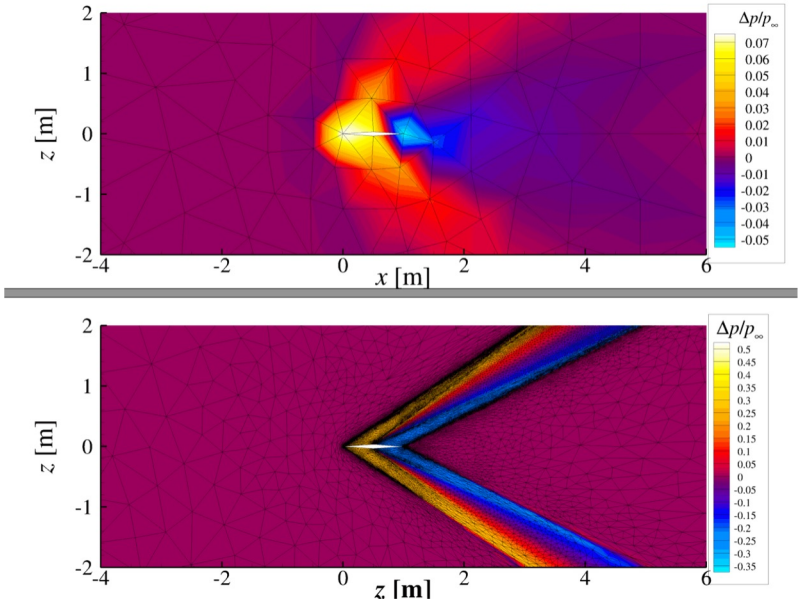

Fig. 2. FUN3D diamond airfoil case at Mach 2.0. Adapted for sonic boom propagation. NASA FUN3D Workshop (NF1676L-31914), 2018.

Sonic Boom Prediction Process

- Hypersonic flow-field is predicted with Parabolized Navier-Stokes (PNS) Solver
- Near-field source cylinder is extracted outside region of induced vorticity
- Sonic boom is propagated to the ground via Waveform Parameter Method

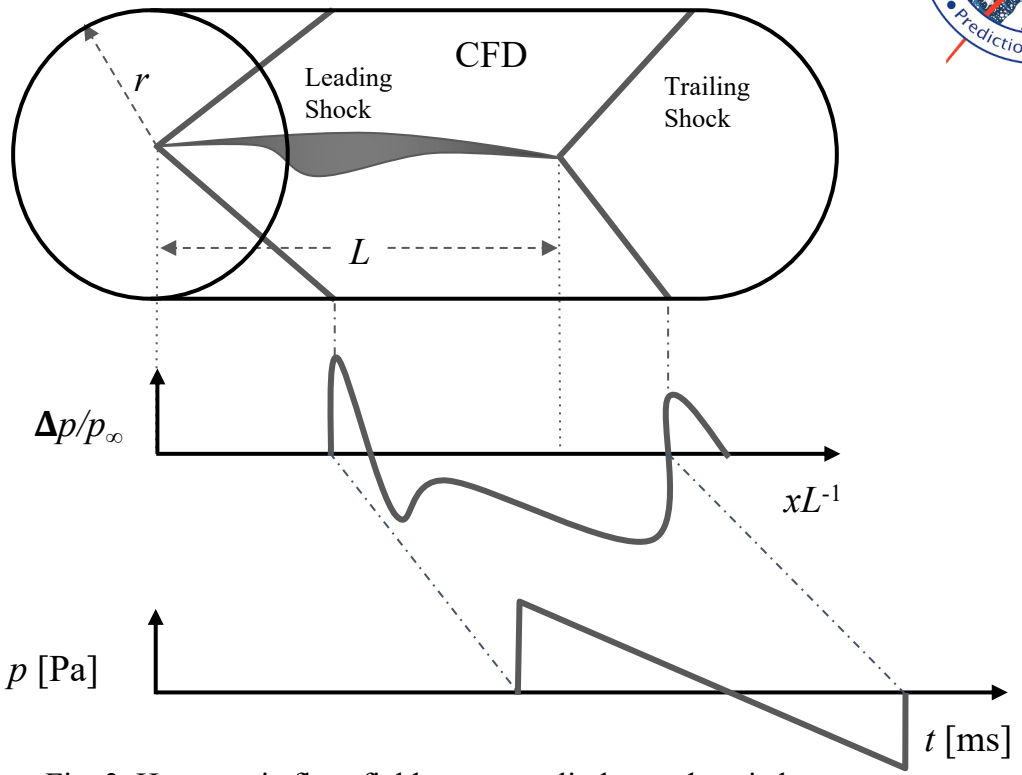

Fig. 3. Hypersonic flow-field, source cylinder, and sonic boom.

Upwind Parabolized Navier-Stokes Solver (UPS)

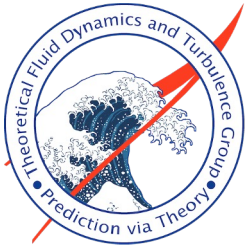

Finite-volume and spatial marching in streamwise direction. Second order upwinding within each cell [3]

$$\frac{\partial \boldsymbol{E}}{\partial \xi} + \frac{\partial \boldsymbol{F}}{\partial \eta} + \frac{\partial \boldsymbol{G}}{\partial \zeta} = 0 \tag{1}$$

$$\left(\frac{\partial \boldsymbol{E}}{\partial \xi}\right)_{i+1} = \frac{1}{\Delta \xi}\left[\boldsymbol{E}^*_{i+1} - \boldsymbol{E}^*_i + \boldsymbol{E}^p(d\boldsymbol{S}_{i+1}, \boldsymbol{U}_{i+2}) - \boldsymbol{E}^p(d\boldsymbol{S}_i, \boldsymbol{U}_{i+1})\right] \tag{2}$$

- $\boldsymbol{E}$, $\boldsymbol{F}$, and $\boldsymbol{G}$ are flux vectors of conserved *mass*, *momentum*, and *energy*
- Separate elliptic portion of *streamwise* flux vector to prevent departure behavior, denoted by superscript p (Vigneron, AIAA, 1978 [4])
- Local iterative approach used for streamwise flow-reversal [5]
- Non-equilibrium flow accounted for via *species continuity* equation and real gas model of Srinivasa [6]

Waveform Parameter Method (WPM)

For sonic boom propagation, three waveform deformation equations for waveform slope, m, static pressure, Δp_i, and segment duration, λ [7]

$$\frac{dm_i}{dt} = c_1 m_i^2 + c_2 m_i \tag{3}$$

$$\frac{d\Delta p_i}{dt} = \frac{1}{2} c_1 \Delta p_i \left(m_i + m_{i-1}\right) + c_2 \Delta p_i \tag{4}$$

$$\frac{d\lambda_i}{dt} = -\frac{1}{2} c_1 \left(\Delta p_i + \Delta p_{i+1}\right) - c_1 m_i \lambda_i \tag{5}$$

Coefficients c_1 and c_2 account for atmospheric variations

- Equations are solved along paths obtained via ray-tracing
- Coalescence of waveform segments are treated as discontinuities

Sonic Boom Validation for WPM NASA/AIAA Sonic Boom Workshop

M_∞ = 1.6, Alt. = 16.76 km, rL^{-1} = 3.13, Reflection Factor =1.90
Maximum relative difference to PCBoom within 8%

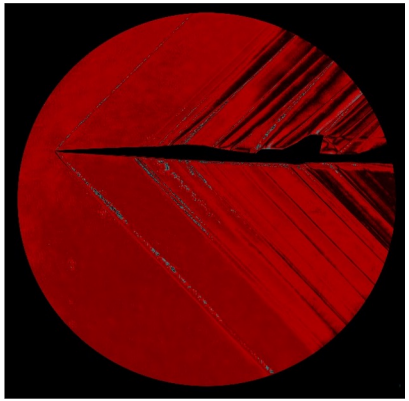

Fig. 4. X-59 low-boom demonstrator [8].

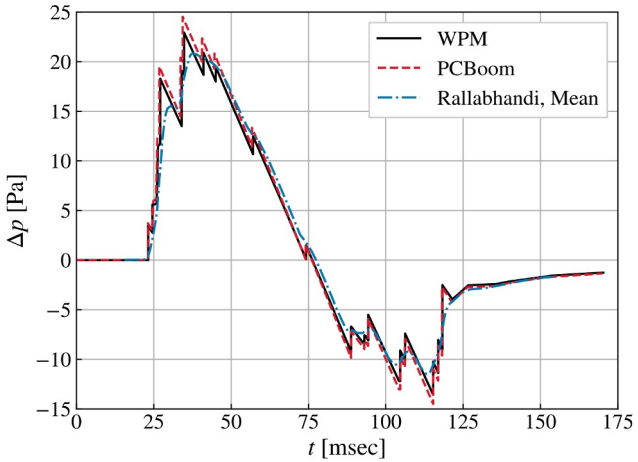

Fig. 5. Axi. body atm. profile 3.

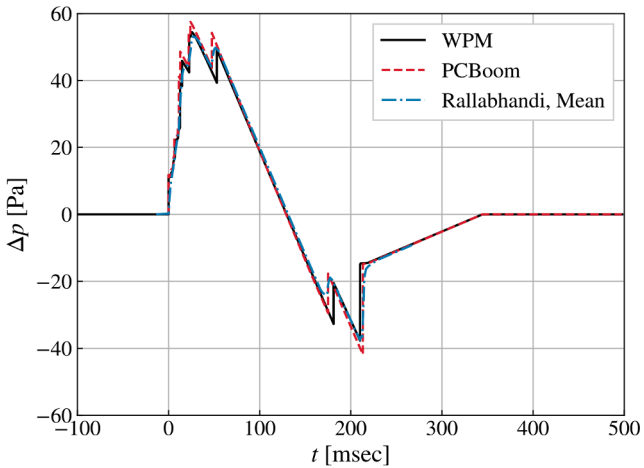

Fig. 6. LM1021. Std. atm.

Sonic Boom Prediction Workshop - NASA - https://lbpw.larc.nasa.gov/ [9]

Sears-Haack Geometry

- The Sears-Haack geometry is chosen due to its simplicity and historical significance

- The Sears-Haack geometry represents the lowest wave drag in supersonic flow, derived via calculus of variations and is defined as

$$S(x) = \frac{16V}{3L\pi}[4x(1-x)]^{3/2} = \pi R_{\max}^2[4x(1-x)]^{3/2} \quad (7)$$

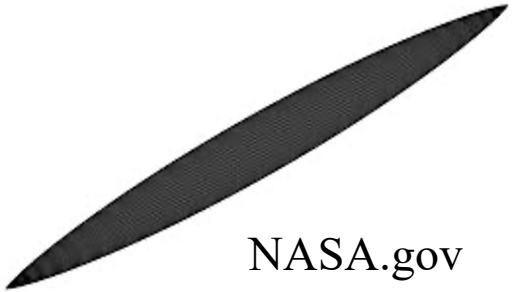

NASA.gov

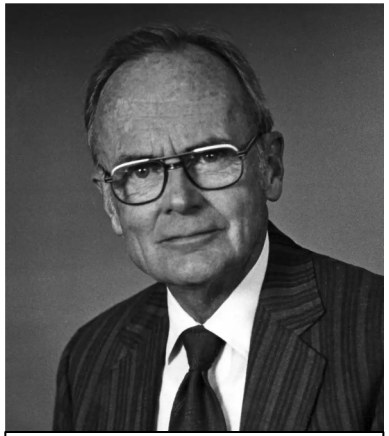

Prof. W. Sears

Jones, R. T., "Theory of Wing-Body Drag at Supersonic Speeds," NACA Report 1284, 8 July 1953 [10].

Sears-Haack Sonic Boom Prediction

- Increased near-field and sonic boom overpressure with viscous stress tensor on average by 15.7% and 8.49%, respectively
- $M_\infty = 7.0$, $p_\infty = 12.13$ kPa, $\rho_\infty = 0.1948$ kg m^{-3}, $T_\infty = 217.0$ K, Alt. = 15.85 km
- Standard Atmosphere, Ground reflection factor = 1.9

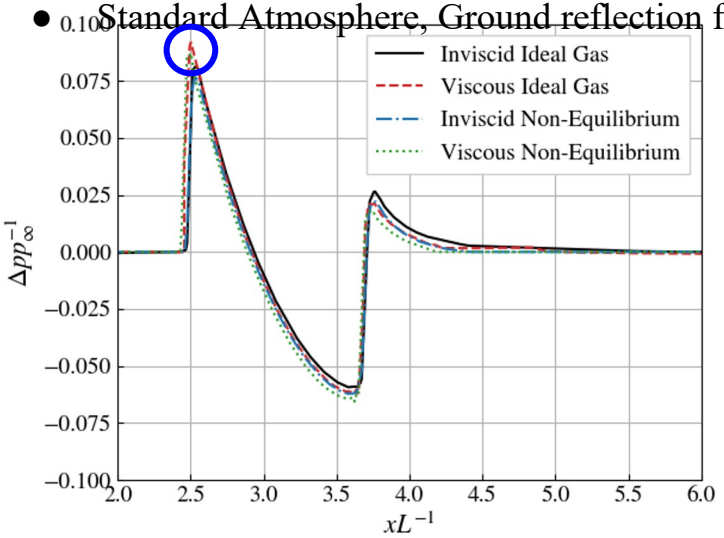

Fig. 7. Near-field signature at $rL^{-1} = 0.3937$.

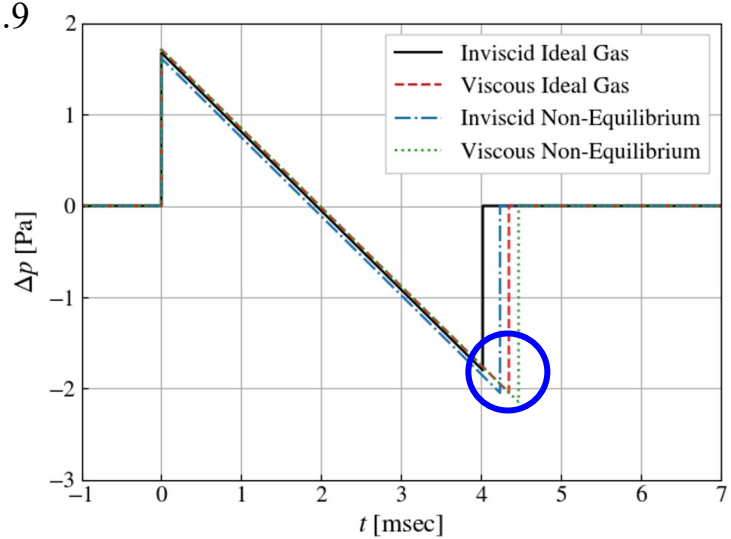

Fig. 8. Ground waveform.

Sound Pressure Level and Overpressures

- Ground waveform SPL shows approximate log-linear relation
- Linear increase in boom overpressure with M_∞
- Negative SPL frequency shift in viscous and non-equilibrium cases due to increased duration and increased viscous overpressure

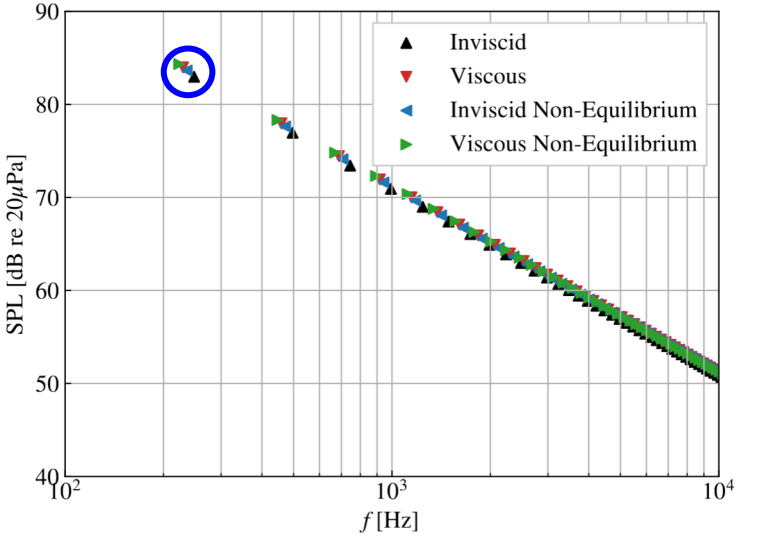

Fig. 9. Ground SPL at $M_\infty = 7.0$.

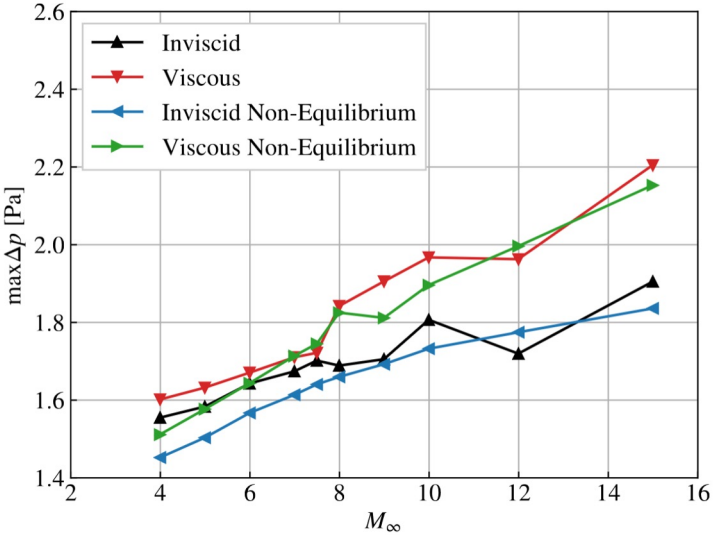

Fig. 10. Sonic boom overpressures across M_∞.

Boundary Layer Impact on Near-Field

- Increase boundary layer displacement thickness distributes P-M expansions over a farther distance
- Less interaction between Prandtl-Meyer

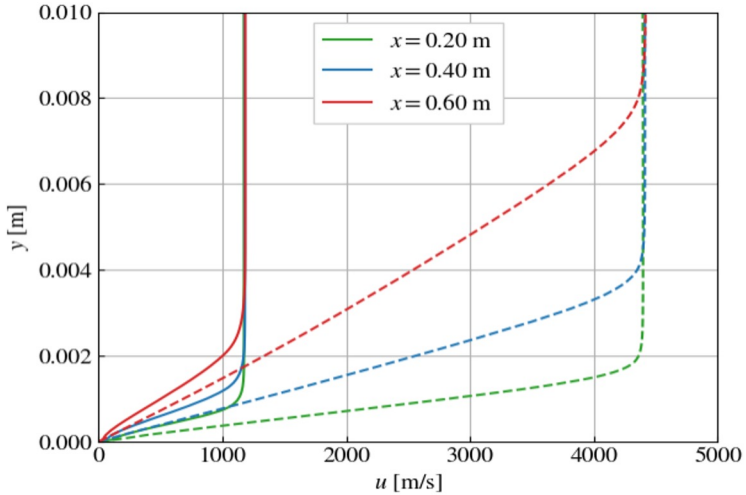

Fig. 11. Boundary layer profiles extracted at $M_\infty = 4.0$ (solid) and $M_\infty = 15.0$ (dashed).

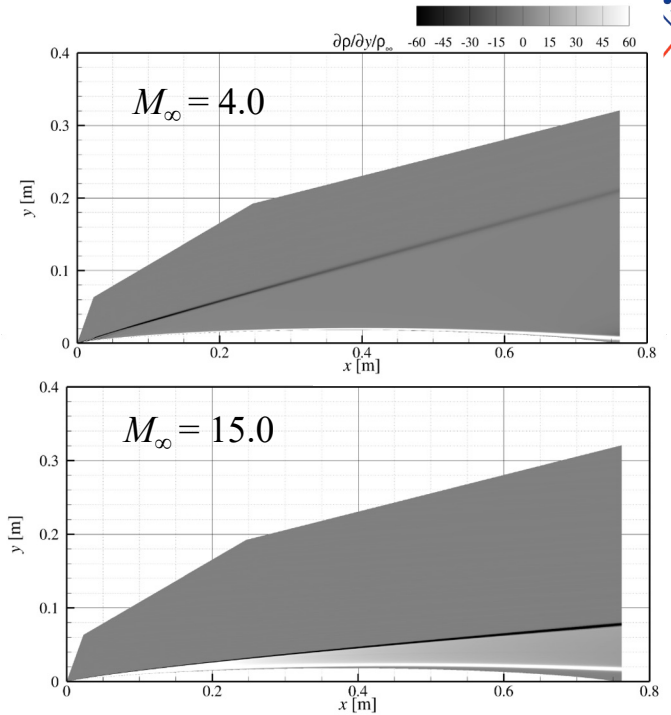

Fig. 12. Numerical schlieren of Sears-Haack body at $M_\infty = 4.0$ (top) and 15.0 (bottom).

HIFiRE-5

- The HIFiRE-5 hypersonic test geometry modeled as elliptic conic sections
- The purpose of its developments was to understand flight behavior in the hypersonic regime
- The stagnation point features a 2:1 elliptical cross-section and converges to a circular section at the end of the forebody

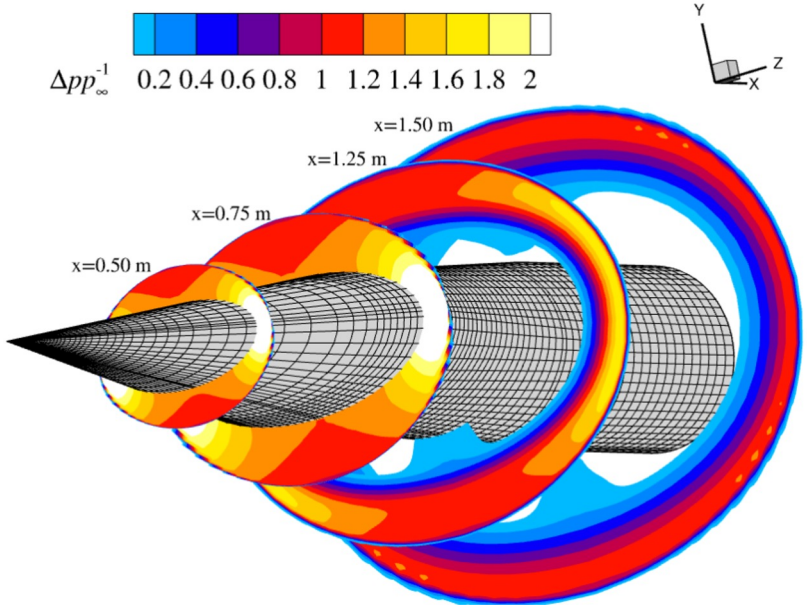

Fig. 13. Contours of pressure coefficient at M_∞ = 7.0.

HIFiRE-5 Near-Field Prediction

- Decrease in overpressure by 3.6 %, on average with non-equilibrium flow
- Near-field signatures are extracted at $rL^{-1} = 0.20$
- Noticeable second pressure rise in $M_\infty = 5.0$ and 6.0 cases

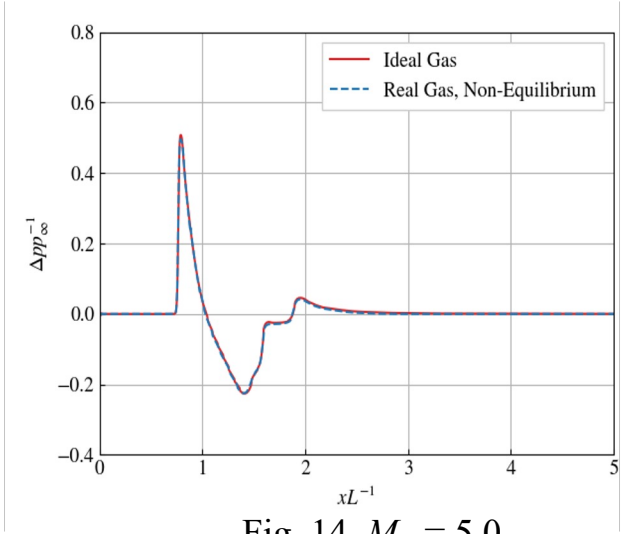

Fig. 14. $M_\infty = 5.0$.

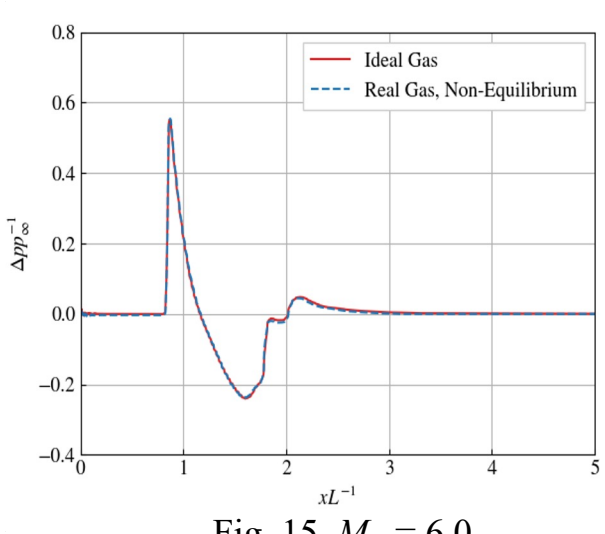

Fig. 15. $M_\infty = 6.0$.

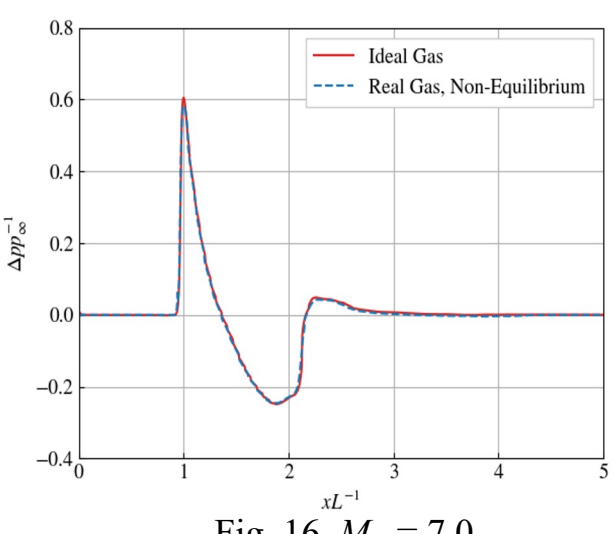

Fig. 16. $M_\infty = 7.0$.

HIFiRE-5 Sonic Boom Prediction

- Increased sonic boom duration causes negative SPL frequency shift
- p_∞ = 12.13 kPa, ρ_∞ = 0.1948 kg m^{-3}, T_∞ = 217.0 K, Alt. = 15.8 km
- Standard Atmosphere, Ground reflection factor = 1.9

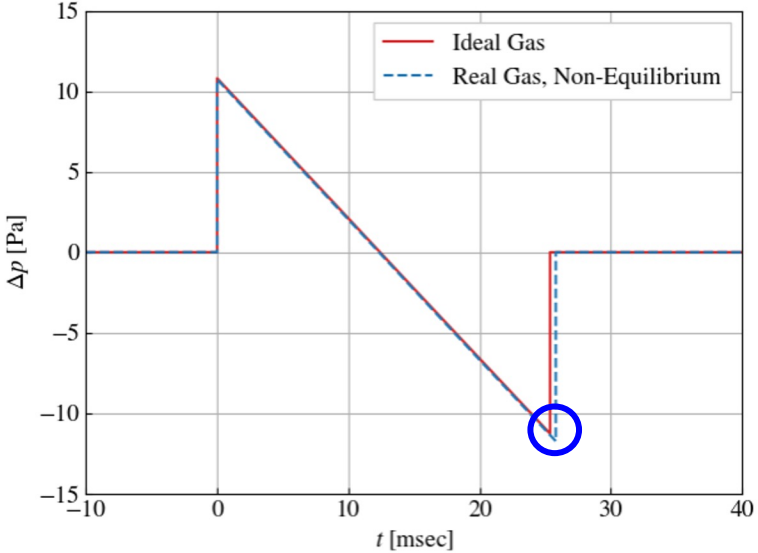

Fig. 17. Sonic boom at the ground at M_∞ = 7.0.

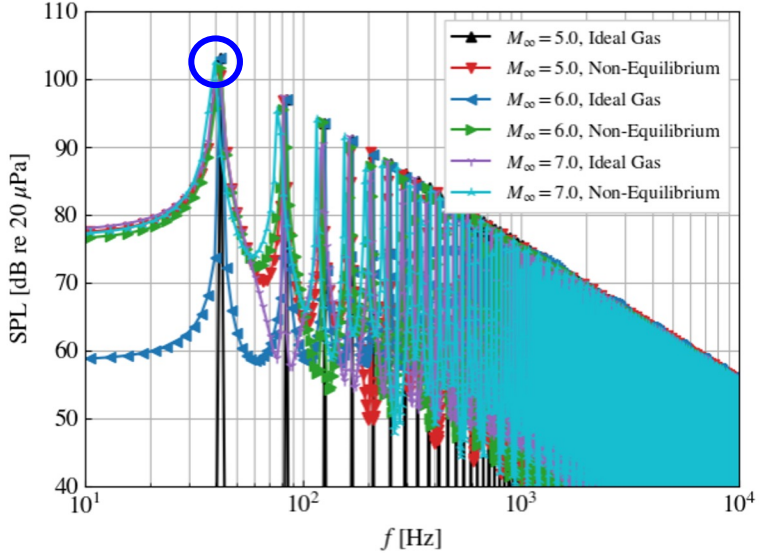

Fig. 18. SPL at the ground.

Power Law Waverider

- Power law waveriders are derived using the two-dimensional power law equations: y_p , y_l and y_u .
- A constant θ ensures a planar shock radiates from the leading edge
- $A = 0.66$ m
- $\beta = 7.0$ deg.
- $\theta = 7.0$ deg.
- $n = 0.50$
- $B = A/\tan^n\beta$
- $L = 50.0$ cm

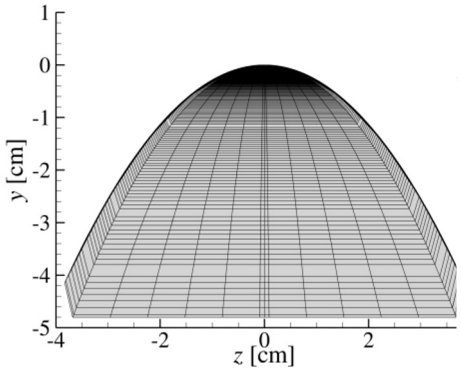

Fig. 19. Front view.

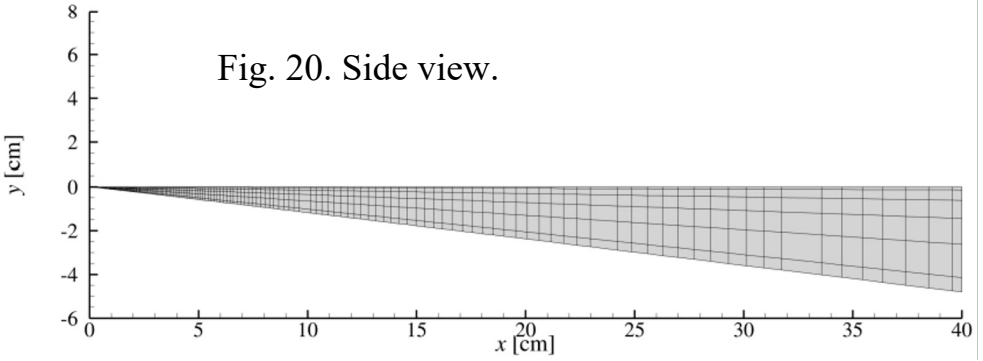

Fig. 20. Side view.

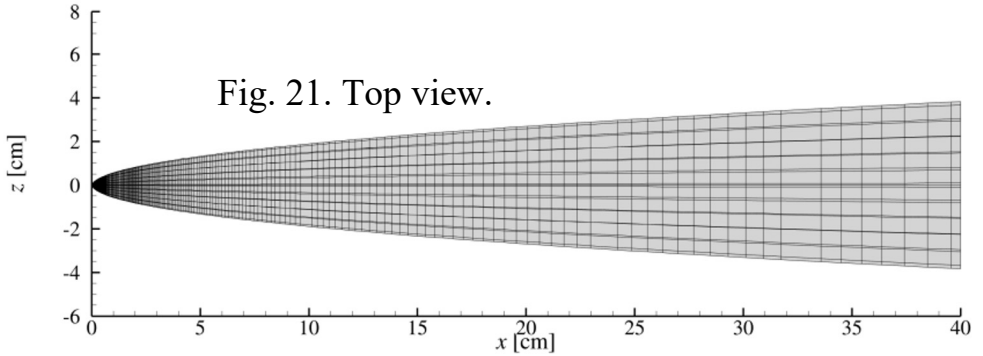

Fig. 21. Top view.

Power Law Waverider

- Equating θ and β yields a flat-bottom configuration.
- The top surface, or freestream surface, theoretically produces no increase in pressure and does not contribute to the lift.

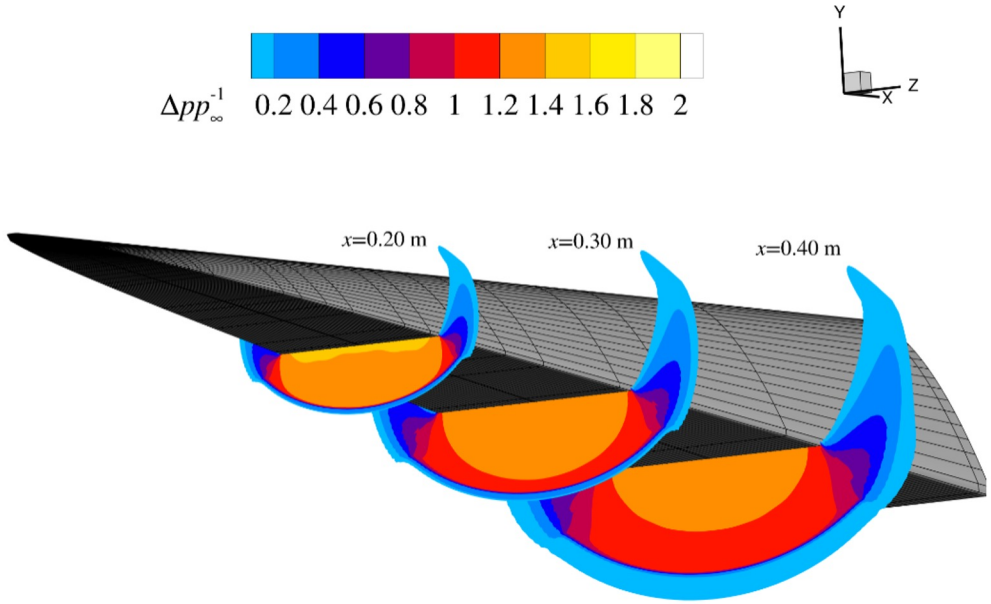

Fig. 22. Contours of pressure coefficient at M_∞ = 7.0 and zero angle-of-attack.

Power-Law Near-Field Prediction

- Decrease in overpressure by 6.3 %, on average with non-equilibrium flow
- Near-field signatures are extracted at $rL^{-1} = 0.20$
- Noticeable second pressure rise in $M_\infty = 5.0$ and 6.0 cases

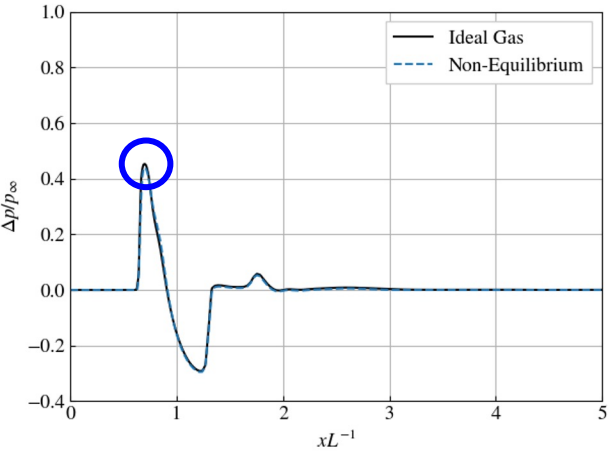

Fig. 23. $M_\infty = 5.0$.

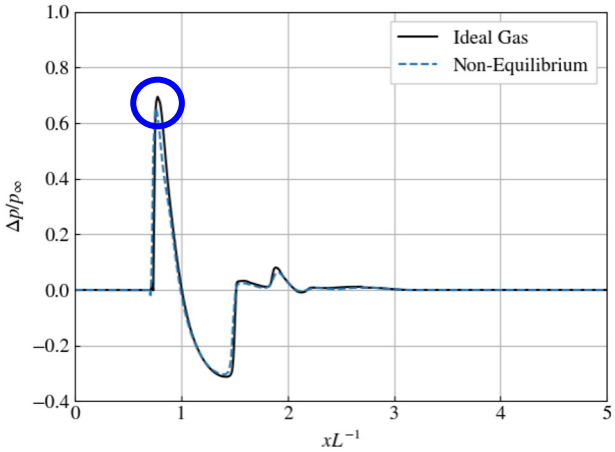

Fig. 24. $M_\infty = 6.0$.

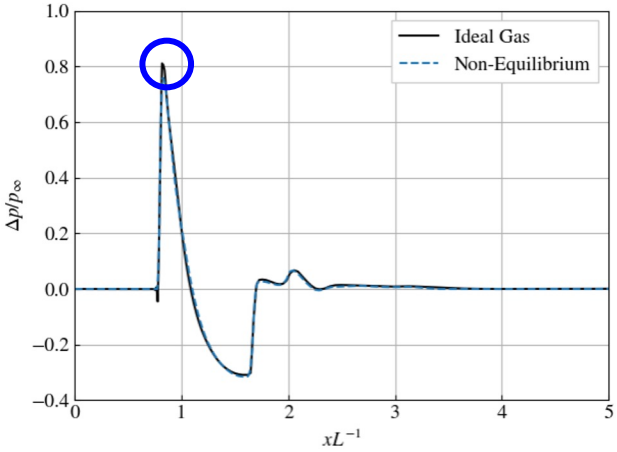

Fig. 25. $M_\infty = 7.0$.

Power-Law Near-Field Prediction

- Negative SPL frequency shift due to increased sonic boom duration
- p_∞ = 12.13 kPa, ρ_∞ = 0.1948 kg m^{-3}, T_∞ = 217.0 K, Alt. = 15.8 km
- Standard Atmosphere, Ground reflection factor = 1.9

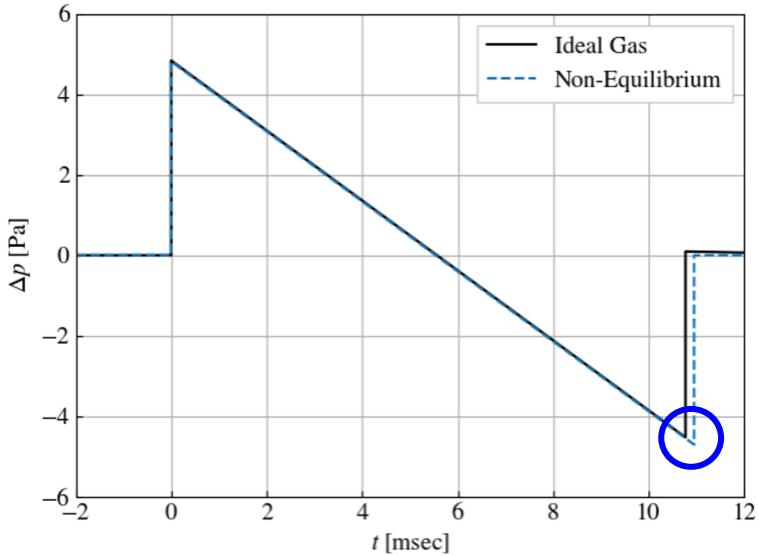

Fig. 26. Sonic boom at the ground at M_∞ = 7.0.

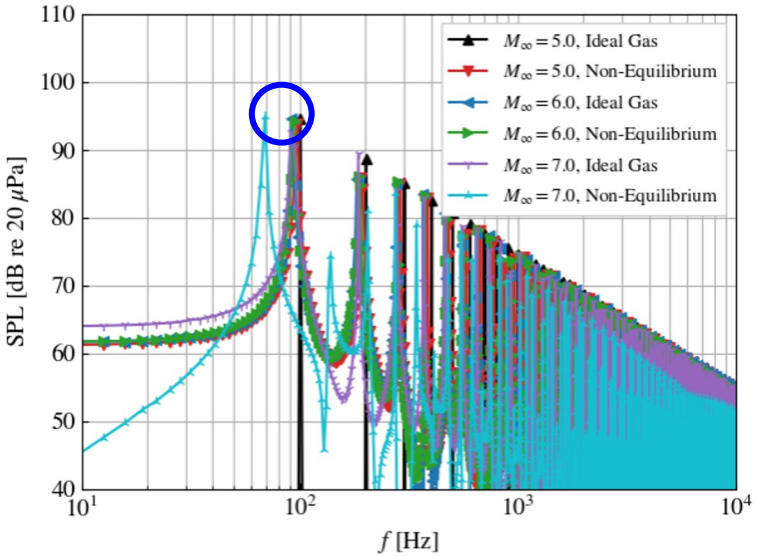

Fig. 27. SPL at the ground.

Conclusion

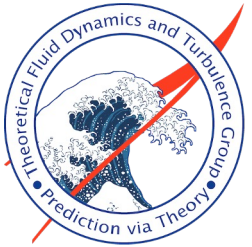

- We present a fully-parabolized prediction approach for the hypersonic near-field and sonic boom
- The viscous stress tensor and non-equilibrium assumption are essential for accurate hypersonic sonic boom prediction
- Including the viscous stress tensor in the solution process increased predicted near-field and sonic boom overpressure by 15.7% and 8.49%, respectively
- In the future, the effect of real atmospheric disturbances on second mode hypersonic instability and turbulent transition will be studied

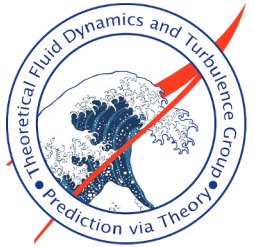

Thank You.

Christian B. King, Univ. Florida Aerospace, christianking@ufl.edu

References

[1] Carlson, H. and Maglieri, D.“Review of Sonic-Boom Generation Theory and Prediction Methods,” Acoustical Society of America, Vol. 51, No. 2C, 1 Feb, 1972, pp 675–685. https://doi.org/10.1121/1.1912901.

[2] Park, M. A., “Adjoint-Based, Three-Dimensional Error Prediction and Grid Adaptation,” AIAA Journal, Vol. 42, No. 9, 2004, pp. 1854–1862. doi:10.2514/1.10051.

[3] Lawrence, S. L., Tannehill, J. C., and Chausee, D. S., “Upwind Algorithm for the Parabolized Navier-Stokes Equations,” AIAA Journal, Vol. 27, No. 9, 1989, pp. 1175–1183. doi:10.2514/3.10243.

[4] Vigneron, Y .,Tannehill, J., and Rakich, J., “Calculation of Supersonic Viscous Flow over Delta Wings with Sharp Subsonic Leading Edges,” 11th Fluid and Plasma Dynamics Conference, American Institute of Aeronautics and Astronautics, AIAA Paper 1978-1137, 1978. doi:10.2514/6.1978-1137.

[5] Miller, J. H., Tannehill, J. C., and Lawrence, S. L., “Parabolized Navier-Stokes Algorithm for Solving Supersonic Flows with Upstream Influences,”AIAA Journal, Vol. 38, No. 10, 2000, pp. 1837–1845. doi:10.2514/2.865.

[6] Tannehill, J., Buelow, P., Ievalts, J., and Lawrence, S., “A Three-Dimensional Upwind Parabolized Navier-Stokes Code for Real Gas Flows,” 24th Thermophysics Conference, American Institute of Aeronautics and Astronautics, AIAA Paper 1989-1651, 1989. doi:10.2514/6.1989-1651.

[7] Thomas, C. L., “Extrapolation of Sonic Boom Pressure Signatures by the Waveform Parameter Method,” NASA TN D-6832, 1972.

[8] Doebler, W.,” Simulations and Case Study of X-59 Low-Booms Propagated Through Measured Atmospheric Profiles,” Acoustical Society of America, 11 December 2020, 42 (1), 022004. https://doi.org/10.1121/2.0001448

[9] Rallabhandi, S. K., and Loubeau, A., “Summary of Propagation Cases of the Second AIAA Sonic Boom Prediction Workshop,” Journal of Aircraft, Vol. 56, No. 3, 2019, pp. 876–895. doi:10.2514/1.c034805.

[10] Jones, R. T., “Theory of Wing-Body Drag at Supersonic Speeds,” NACA Report 1284, 8 July, 1953.